Computer-generated image hologram

Takeshi Yamaguchi* **and Hiroshi Yoshikawa**

Department of Electronics and Computer Science, College of Science and Technology, Nihon University 7-24-1 Narashinodai, Funabashi-shi, Chiba 274-8501, Japan

**Corresponding author: yamaguchi@ecs.cst.nihon-u.ac.jp*

Received July 26, 2011; accepted September 15, 2011; posted online November 25, 2011

We investigate the computer-generated hologram with full parallax and which can be reconstructed with white light. The object of the hologram is processed from three-dimensional computer graphics polygon data and has shaded surface for hidden surface removal. The optically reconstructed image from the printed hologram is evaluated.

OCIS codes: 090.0090, 090.1760.
doi: 10.3788/COL201109.120006.

The hologram has three-dimensional (3D) information such as the binocular parallax, the convergence, and accommodation. Therefore, the reconstructed image of the hologram provides natural spatial effect. In particular, the viewer gets strong dimensional impression when the image is popping up from the hologram plane.

We have been studying computer-generated hologram (CGH), whose interference fringes are calculated on the computer. We have also developed the output device of the CGH, which is called fringe printer. The improved fringe printer[1] is able to provide the 0.44 μm pitch and over 100 Gpixels hologram. Using this fringe printer, we have printed the computer-generated Fresnel hologram[1] (CGFH), the computer-generated rainbow hologram[2] (CGRH), the computer-generated cylindrical hologram[3] (CGCH), the computer-generated disk hologram[4] (CGDH), and the computer-generated alcove hologram[5] (CGAH). There are also some published papers about printed CGH[6−9]. However, most CGHs are of Fresnel type[7−9]. Therefore, CGHs require the laser or the single color LED for the illumination. Reference [6] can be reconstructed by white light. However, this CGH only has the horizontal parallax. Since the pixel pitch of the CD-R is not enough for the 3D CGH, the viewing angle is not enough. In addition, proper hidden surface removal is necessary when the pixel pitch of the output device becomes fine.

In this letter, we investigate the image type CGH, which is the output of the fringe printer. We propose the modified hidden surface removal method for the image type CGH. We calculate and output the CGH of the shaded object processed from the computer graphics polygon data. The reconstructed images show proper hidden surface removal and full parallax.

The rigorous calculation method described in this section is based on an exact optical model. The object to be recorded is approximated as a collection of self-illuminated points[10], and located at a certain point in a system of Cartesian coordinates. The calculation geometry of the hologram is shown in Fig. 1.

The hologram is located on the xy-plane, and the observer's side takes positive value of the z-axis. The location of the ith object point is specified as (x_i, y_i, z_i). Each point has real-valued amplitude a_i and relative phase ϕ_i. The complex amplitude $\mathbf{O}(x, y)$ on the hologram is determined from the superposition of the object wavefronts by

$$\mathbf{O}(x,y) = \sum_{i=1}^{N} \frac{a_i}{r_i} \exp[\mathrm{j}(kr_i + \phi_i)], \tag{1}$$

where N is the number of object points. The wave number k is defined as $k = 2\pi/\lambda$, where λ is the free-space wavelength of the light. The oblique distance r_i between the ith object point and the point (x, y) on the hologram is defined as

$$r_i = \sqrt{(x - x_i)^2 + (y - y_i)^2 + z_i^2}. \tag{2}$$

If the reference beam is collimated, the complex amplitude of the reference beam $\mathbf{R}(x, y)$ is represented as

$$\mathbf{R}(x,y) = a_{\mathrm{R}} \exp(\mathrm{j}ky \sin\theta_{\mathrm{ref}}), \tag{3}$$

where a_{R} is the real-valued amplitude and θ_{ref} is the incident angle of the reference beam. The total complex amplitude on the hologram plane is the interference of the object beam and the reference beam represented as $\mathbf{O}(x, y)$+$\mathbf{R}(x, y)$. The total intensity pattern,

$$I(x,y) = |\mathbf{O} + \mathbf{R}|^2 = |\mathbf{O}|^2 + |\mathbf{R}|^2 + 2\mathrm{Re}\{\mathbf{O}\mathbf{R}^*\}, \tag{4}$$

is a real physical light distribution on the hologram, where Re{**C**} takes the real part of the complex number **C**, and $\mathbf{R}^*$ means the conjugate of **R**. The first term represents the object self-interference and the second term

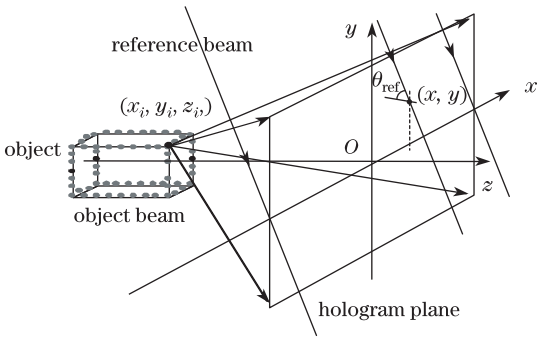

Fig. 1. Model to calculate the Fresnel hologram.

is the reference beam intensity. The third term is the interference of the object beam and the reference beam that contains the holographic information.

Since the holographic information is contained only in the third term of Eq. (4), we can substitute I to

$$I_{\rm b}(x,y)=\sum_{i=1}^{N}\frac{a_i}{r_i}\cos[kr_i+\phi_R(x,y)+\phi_i], \qquad (5)$$

where $\phi_{\rm R}$ is the phase of the reference beam.

Lucente has named $I_{\rm b}(x,y)$ as the "bipolar intensity", because it contains negative and non-negative values[10,11]. The bipolar intensity corresponds to incoherent holography, and the fringes can be computed by real numbers only, although complex numbers must be used to obtain coherent holography in Eq. (4). With this modification, a speed-up factor of 2 is reported[11].

Figure 2 shows the configuration to record the image hologram[12] optically. Since the image of the object is located very close to or even on the hologram, the chromatic aberration caused by the difference of wavelength becomes small. Therefore, the hologram can reconstruct images with white light. However, the image blur increases when the distance from the hologram plane increases, thus it is difficult to reconstruct the image with large depth by white light. In addition, the diffracted angles vary with wavelength; it can be observed that when the viewer moves up and down, the reconstructed image sometimes shows color changes if the image size is huge. However, these problems can be solved by using the laser or LED as an illumination source. The view zone of the image hologram depends on the aperture of lens and imaging position as shown in Fig. 2. Therefore, to expand the view zone, we should use small F number lens with larger aperture and shorter focal length.

The calculation of the image hologram is basically the same as the Fresnel hologram. However, there are two things to be considered. The first is the sign of the phase kr_i in Eq. (5). If the ith object point is located in front of the hologram plane, or $z_i>0$, then the phase term should be $-kr_i$. The second is the divergence of the fringe when r_i gets close to zero. If r_i takes a very small value, the value of r_i^{-1} in Eq. (5) becomes large, and this affects the fringes from other object points. One solution to avoid this problem is by adding small positive value ϵ to r_i. With these modifications, Eq. (5) can be rewritten as

$$I_{\rm b}(x,y)=\sum_{i=1}^{N}\frac{a_i}{r_i+\epsilon}\cos[s(z_i)kr_i+\phi_{\rm R}(x,y)+\phi_i], \qquad (6)$$

where $s(z_i)$ is a function which returns 1 when z is negative or the point image is located behind the hologram, otherwise returns.

When the viewing angle of the CGH becomes large, the object data should be processed by proper hidden surface removal. If this process is not proper, there will be problems such as overlapping object points and the appearance of occlusion holes. Therefore, we prepared a set of object data from different viewpoints. The object data format for the calculation consists of 3D coordinates, the amplitude, and the phase of the point light sources. The object data are generated from the intensity image and the depth image obtained by the computer graphics software[13]. At first, we render perspective images of each viewpoint from outside the object, as shown in Fig. 3. The depth information is then added to the images, and these become the object data. For the Fresnel hologram, the hologram plane can be set to be the same as the camera plane. Therefore, each hologram data from each camera can be used to calculate small elemental holograms.

For the calculation of the image type CGH, the hologram plane and the camera plane are located at different places, as shown in Fig. 4. Like the camera plane, the hologram plane is also divided into small segments. For each hologram segment, all object data are used for calculation. The camera plane is assumed as an array of virtual windows[14] corresponding to each camera. Therefore, the object data are used for calculation

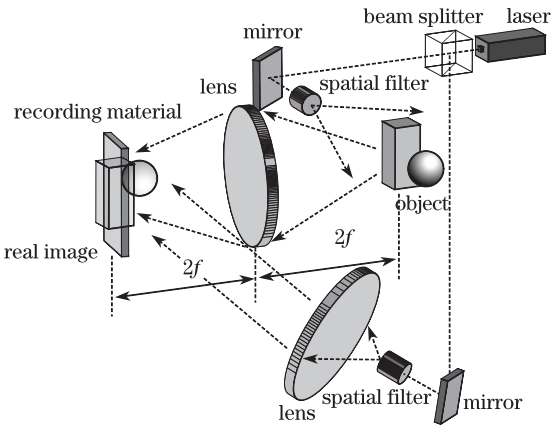

Fig. 2. Optical configuration to record an image hologram.

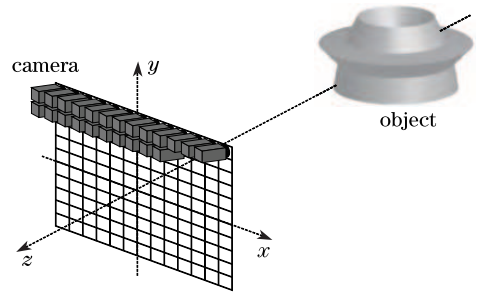

Fig. 3. Process to create perspective images from different viewpoints.

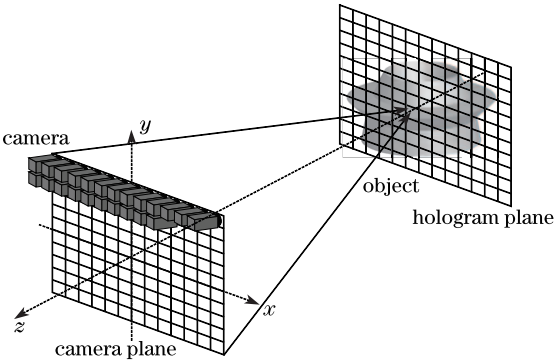

Fig. 4. Relation between the camera plane and the hologram plane.

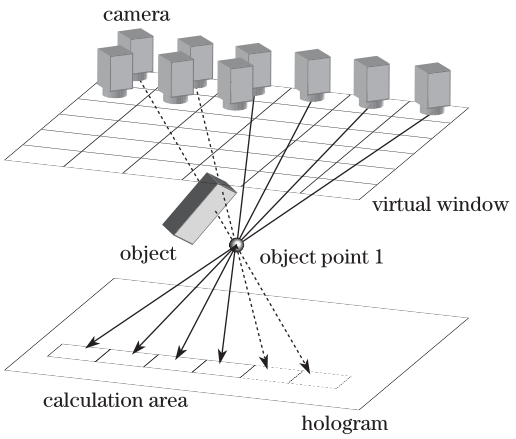

Fig. 5. Relation between the segmented virtual window and the calculation area.

Table 1. Parameters of the Fringe Printer

Fringe Printer	Value
Moving Area (mm^2)	200×200
Focal Length (L3) (mm)	200
Focal Length (L4) (mm)	12.5
Demagnification Rate	1/16
Wavelength (laser) (nm)	473
LCoS	Value
Number of pixels (pixel)	1 920×1 080
Pitch (μm)	7.0
Grayscale Level (bit)	8

Table 2. Parameters of the Calculated Hologram

Parameter of the Hologram	Value
Number of Pixels (pixel)	250 000×160 000
Size (mm^2)	110×70.4
Pitch (μm)	0.44
Wavelengths (nm)	525
Incident Angle of Reference Beam (deg.)	20
Segment Size (pixel)	1 920×1 080
Virtual Window Size (m)	1.15×0.31
Position of the Virtual Window (m)	(0, 0, 1.0)
Partition number of Virtual Window	31×21
Number of Object Points (ave.)	20 000

when the light passes the corresponding virtual window (Fig. 5).

For printing the CGH, we used the fringe printer that consists of a laser, an x-y stage, and a liquid crystal on silicon (LCoS) as a spatial light modulator, as shown in Fig. 6. A fractional part of the entire holographic fringe is displayed on the LCoS, and the demagnified image of it is recorded on a holographic plate. The plate is then translated by the x-y stage to write the next part of the fringe. Table 1 shows the fringe printer's parameters.

Table 2 shows the parameters of the CGH proposed in this letter. We used our fringe printer to record the fringe pattern.

For the calculation, the object shown in Fig. 7 was used, which consists of about 20 000 points for each camera. The character is placed ±22.7 mm from the hologram plane. The calculation time is approximately 20 h with one PC (CPU: Intel Core(TM) i7 980X, 3.33 GHz). The printing time is about 10 h.

Figures 8 and 9 show the numerically-simulated images. Figure 8 is calculated by object data made from a single camera position. Figure 9 is calculated with the modified hidden surface removal method as discussed above. As shown in Figs. 8(a) and (c), since the fringe pattern is calculated by object data converted from a single camera, the viewer recognizes overlapping object points and the appearance of occlusion holes. In

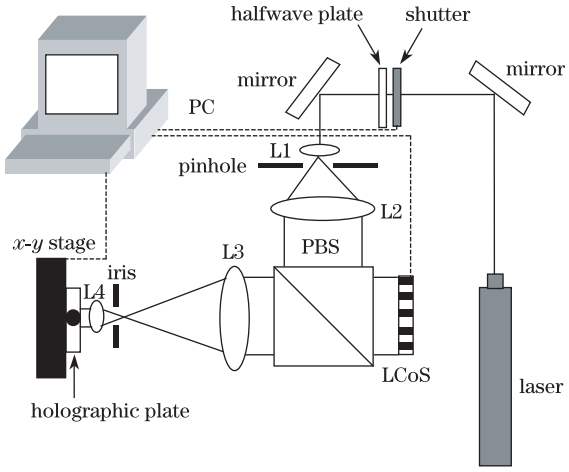

Fig. 6. Schematic of the fringe printing system.

Fig. 7. Perspective image of the recorded object.

(a) Left (b) Center (c) Right

Fig. 8. Numerical reconstructions of the fringe pattern with an object converted from a single camera.

(a) Left (b) Center (c) Right

Fig. 9. Numerical reconstructions of the fringe pattern with object data from 651 cameras.

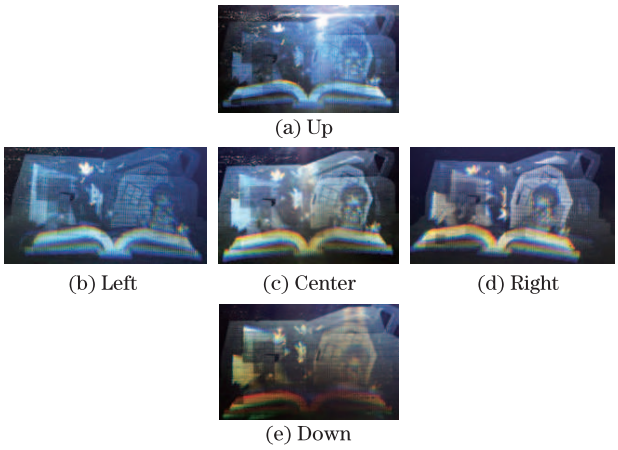

(a) Up

(b) Left (c) Center (d) Right

(e) Down

Fig. 10. Reconstructed image from various viewpoints.

Table 3. Measurement of the Viewing Angle

Type of Value	Horizontal (deg.)	Vertical (deg.)
Measured Value	47.2	26.6
Theoretical Value	42.1	28.3

contrast, with the modified hidden surface removal method, the simulated image shows properly from every viewing position as shown in Fig. 9.

Figure 10 shows the optically reconstructed images of the CGH from various viewpoints. We used the VRP-M manufactured by Slavich as a recording material. The CGH is illuminated by the collimated light from the white LED. The reconstructed images show the hidden surface removal properly. The parallax of the reconstructed images are also confirmed when the observing point is changed. However, some holes which are not of the occlusion type remained. To solve the divergence of the fringe, we added the value ϵ in Eq. (6). However, the calculated fringe size is small when the reconstructed object point is close to the hologram, and the decision of the value of ϵ is difficult. Therefore, the reconstructed image, which is close to the hologram, is not bright and could not be observed. Additionally, since the calculation amount is very large, the fringe pattern is divided into small segments (17×13) when the fringe pattern is calculated. To increase the contrast of the reconstructed image, each segment of the fringe pattern is normalized individually. Therefore, the reconstructed image shows brightness inhomogeneity.

We also measured the viewing angle of the CGH as shown in Table 3. The viewing angle is defined as the angle at which the viewer can observe the reconstructed image. In comparison with the theoretical value, the measured value becomes lager in the horizontal view but smaller in the vertical view.

In conclusion, we investigate the image type CGH. Based from the reconstructed images, it is confirmed that proper hidden surface removal is applied to the recorded object and that the CGH shows full parallax.

The authors thank Dr. Tomohiko Fujii, Mr. Kaname Saito, Mr. Tadashi Miyahara, and Ms. Yayoi Nakaguchi for their help in making the image hologram. Part of this work was supported by the Futaba Electronics Memorial Foundation.

References

1. H. Yoshikawa and T. Yamaguchi, Chin. Opt. Lett. **7,** 1079 (2009).
2. Y. Nakaguchi, T. Yamaguchi, and H. Yoshikawa, in *Proceedings of International Conference on 3D System and Applications 2010* 111 (2010).
3. T. Yamaguchi, T. Fujii, and H. Yoshikawa, Appl. Opt. **47,** D63 (2008).
4. T. Yamaguchi, T. Fujii, and H. Yoshikawa, Appl. Opt. **48,** 34 (2009).
5. T. Yamaguchi, H. Ozawa, and H. Yoshikawa, Proc. SPIE **7957,** 795719 (2011).
6. Y. Sakamoto, M. Morishima, and A. Usui, Proc. SPIE **5290,** 42 (2004).
7. K. Matsushima, S. KobayashiD, and H. MiyauchiD, Proc. SPIE **6136,** 347 (2006).
8. A. Kashiwagi and Y. Sakamoto, in *Proceedings of Digital Holography and Three-Dimensional Imaging on CD-ROM* DWB7 (2007).
9. K. Matsushima and S. Nakahara, Appl. Opt. **48,** H54 (2009).
10. J. P. Waters, Appl. Phys. Lett. **9,** 405 (1966).
11. M. Lucente, J. Election. Imaging **2,** 28 (1993).
12. L. Rosen, Appl. Phys. Lett. **9,** 337 (1966).
13. T. Fujii and H. Yoshikawa, in *Digital Holography and Three-Dimensional Imaging, Security and Environmental Analysis on CD-ROM* DWB3 (2007).
14. T. Yamaguchi, G. Okabe, and H. Yoshikawa, Opt. Eng. **46,** 125801 (2007).